PCCP

Accepted Manuscript

ROYAL SOCIETY OF CHEMISTRY

www.rsc.org/pccp

Journal Name

RSCPublishing

ARTICLE

Understanding chemical expansion in perovskite-structured oxides

Cite this: DOI: 10.1039/x0xx00000x

Dario Marrocchelli[a,b,c,†,*], Nicola H. Perry[c,d,†] and Sean R. Bishop[c,d]

Received ooth January 2012,
Accepted ooth January 2012

DOI: 10.1039/x0xx00000x

www.rsc.org/

In this work, chemical expansion in perovskite oxides was characterized in detail, motivated, inter alia, by a desire to understand the lower chemical expansion coefficients observed for perovskites in comparison to fluorite-structured oxides. Changes in lattice parameter and in local atomic arrangements taking place during compositional changes of perovskites, i.e., stoichiometric expansion, were investigated by developing an empirical model and through molecular dynamics and density functional theory atomistic simulations. An accurate empirical expression for predicting lattice constants of perovskites was developed, using a similar approach to previous reports. From this equation, analytical expressions relating chemical expansion coefficients to separate contributions from the cation and anion sublattices, assuming Shannon ionic radii, were developed and used to isolate the effective radius of an oxygen vacancy, r_v. Using both experimental and simulated chemical expansion coefficient data, r_v for a variety of perovskite compositions was estimated, and trends in r_v were studied. In most cases, r_v was slightly smaller than or similar to the radius of an oxide ion, but larger than in the fluorite structured materials. This result was in good agreement with the atomistic simulations, showing contractive relaxations of the closest oxide ions towards the oxygen vacancy. The results indicate that the smaller chemical expansion coefficients of perovskites vs. fluorites are largely due to the smaller change in cation radii in perovskites, given that the contraction around the oxygen vacancy appears to be less in this structure. Limitations of applicability for the model are discussed.

Introduction

Perovskite-structured materials display a series of electrical, magnetic, piezoelectric, optical, catalytic, and magnetoresistive properties, critical to a variety of technological applications, such as solar cells [1], fuel cells [2], steam electrolysis [3], resistive memories [4–6], and catalysis [7,8]. Point defects play an important role in influencing the above properties, and "defect engineering" provides a way to change/tailor these properties.[9] For example, Sr and Mg are commonly substituted for La and Ga in $(La,Sr)(Ga,Mg)O_{3-\delta}$ to create oxygen vacancies (δ) by charge compensation, thereby dramatically increasing the oxide-ion conductivity of this material and making it a usable solid oxide fuel cell electrolyte [10–12]. In addition to directly modifying electrical properties, these point defects also can significantly modify the lattice parameter, a phenomenon known as chemical expansion [13]. As discussed below, chemical expansion can lead to mechanical instabilities of the device under operation, structural changes, and corresponding indirect changes in the electrical and electrochemical properties. In this paper, the origins of chemical expansion in perovskite materials are examined using empirical relationships applied to available experimental data and with aid from atomistic level calculations.

Chemical expansion refers to the spatial dilation of a material that occurs upon changes in its composition and can be further broken down into two types: (1) *stoichiometric expansion* following a gradual change in lattice parameter with change in composition (i.e., stoichiometry) and (2) *phase change expansion* describing a change in phase with change in

composition [13]. The former case largely impacts materials with small changes in ion concentration (e.g. mixed conducting electrodes for SOFCs) while the latter occurs for larger changes in composition and consequently typically leads to larger expansions (e.g. battery electrodes, hydrogen storage materials) [13]. Though often smaller, stoichiometric expansion (which is largely the focus of this paper) is usually considered detrimental to most technological applications, as it can lead to mechanical instabilities as well as small changes in local and long range order [13–15]. For example, the stoichiometric expansion of the mixed conducting $(La,Sr)(Co,Fe)O_{3-\delta}$ cathode leads to an approximate 50% increase in the total thermo-chemical expansion coefficient upon heating near the ~ 800 ^{o}C operating temperature in air [16,17]. In this case, a stoichiometric expansion coefficient, relating the expansion to the change in chemical species content (e.g., δ: oxygen non-stoichiometry), is commonly defined, though often generically called the chemical expansion coefficient [13,17,18]. Throughout this paper we will use either term.

Recently, authors of this paper have performed an in-depth study of the atomistic causes of this phenomenon in fluorite-structured materials. This investigation was achieved by combining state-of-the-art computational techniques (Density Functional Theory and Molecular Dynamic calculations) with new experimental data from dilatometry and high-temperature XRD experiments [19–21]. Chemical expansion was found to be the result of two competing processes: 1) lattice contraction around an oxygen vacancy (primarily due to electrostatic interactions) and 2) lattice expansion from the change in the cation radius (primarily due to steric effects). Often the latter quantity is much larger (e.g., reduction of Ce^{4+} to Ce^{3+}, or Gd^{3+} or La^{3+} doping in CeO_2), thus resulting in a net expansion. To describe the vacancy-induced contraction, the radius of a vacancy, an empirical parameter describing lattice relaxation, was introduced and shown to be smaller than that of an oxide ion. Recent studies by other investigators also confirmed this finding [22–24]. Interestingly, the magnitude of relaxation around a vacancy was found to be larger in those materials with a host cation that is either significantly smaller (Hf^{4+} and Zr^{4+}) or larger (Bi^{3+}) than cerium, leading to a smaller stoichiometric expansion coefficient [25]. This effect was used as a novel method for reducing the chemical expansion of ceria by partial substitution with zirconia [19].

Chemical expansion in perovskite-based oxides has been extensively characterized by means of experiments, as reviewed by Atkinson and Ramos [15]. One of their interesting findings when summarizing the works of Armstrong et al., Mori et al., and Larsen et al. [26–29] is that (we paraphrase the authors) *the chemical expansion [in perovskite-structured materials] per oxygen vacancy is intrinsically lower than in the fluorite structure*. It would be interesting to provide an explanation for this observation, as this property could, in principle, be used to devise materials with lower chemical expansion. We note that, with the exception of one recent work [22] in which the authors estimate the vacancy radius in acceptor doped $LaGaO_3$, no studies have explicitly addressed this difference. In our paper, we examine the origin of stoichiometric expansion in several perovskite materials and use DFT calculations to provide an atomistic understanding of this phenomenon.

We suggest six factors that can affect stoichiometric expansion coefficients in perovskites as compared to other materials (for example, the fluorite oxides mentioned above):

1) *The different crystalline structure*. Indeed, as we have shown in our previous work, the pattern of ion spatial relaxations around a vacancy influences the final expansion of the material and this process, in turn, is expected to be different in another crystalline structure. For example, in perovskites, usually only one of the two cation sublattices hosts cations undergoing a radius change, as compared to fluorites with just one cation lattice. In the recent work noted above[22], those authors attributed the different oxygen vacancy radius in perovskites vs. fluorites to the "restraining action of A-site lattice on B-site expansion and vice versa." Understanding the nature of these relaxations in perovskite structures is one of the focuses of this paper.

2) *The different chemical formula.* Since perovskites have the general chemical formula $ABO_{3\pm\delta}$, the oxygen vacancies (and consequent reduced cations) created per formula unit will be more dilute vs. fluorites, and so the volumetric expansion per δ will be smaller. In other words, in terms of the volumetric concentration of vacancies, δ is defined differently in the two crystal structures. This effect can be overcome by expressing the volume related property (chemical expansion) as a function of number of defects per volume (i.e. concentration) rather than δ, as described in ref [30], and included for comparison later in this paper.

3) *Subtle symmetry changes during expansion.* While maintaining the perovskite structure, deviations from cubic symmetry – involving tilting of BO_6 octahedra, octahedral distortions, or cation shifts – could occur as the stoichiometry changes, influencing the magnitude of the bulk chemical expansion. Such changes, resulting in anisotropic chemical expansion [31], have been investigated in another publication [32] and will not be a focus here.

4) *The degree of electronic charge localization*, i.e., whether the electrons left behind (when the oxide ions are removed) localize on the cations (ionic/polaronic character) or are delocalized (metallic character). Previously it was shown that charge localization increases the cation radius change upon reduction, leading to a larger chemical expansion [21,32,33]. This paper is mostly limited to materials with a clear ionic character and in which oxygen vacancies are introduced by aliovalent doping rather than reduction.

5) *The presence of magnetic cations.* Spin state impacts local structure, e.g., octahedral distortions, and ionic radii, and therefore may be expected to affect the chemical expansion behavior of perovskites containing magnetic cations that undergo valence state or spin state changes.[34] In the present calculations we limit treatment to non-magnetic cations.

6) *Ordering and defect association at high dopant concentrations*. The role of ordering and defect association should in some cases be considered as another factor affecting

chemical expansion in perovskites [23,35–38], though often this ordering is also related to structural changes [37,38]. In fluorite structures, defect association has been implicated in causing composition-dependent [19,39,40] and temperature-dependent [23] chemical expansion coefficients. The present work focuses on structures without appreciable ordering.

In this paper we provide a detailed atomistic understanding of the factors affecting the chemical expansion coefficient in perovskite-based materials, focusing on factors 1) and 2) above. First we study doped $LaGaO_3$, $LaAlO_3$, and $SrTiO_3$ and show which atomistic factors are responsible for the chemical expansion of these materials. $LaGaO_3$, $LaAlO_3$, and $SrTiO_3$ are chosen for study because they are either cubic or close to cubic, and the ionic radii are well defined, as opposed to many of the multivalent doped materials where aspects such as unknown spin state and charge localization can impact the radii [21,32]. Then we will develop an analytical model that describes the chemical expansion coefficient of these materials in terms of the radii of the ionic species, including the radius of a vacancy. This model will then be applied to data from the literature on a variety of pseudo-cubic perovskite systems.

Methodology

In this work we used both Density Functional theory calculations and Molecular Dynamics simulations based on dipole-polarizable interionic potentials. The details of these techniques have been described in depth in previous publications [20,21,25], where we have also shown how these techniques can provide complementary information. For this reason only a concise description will be given here.

Density Functional Theory

Density Functional Theory calculations were performed with the Vienna Ab-initio Simulation Package (VASP)[41], with the Projector Augmented Wave (PAW) method. We used the Generalized Gradient Approximation (GGA) with the PBE exchange-correlation functional and an energy cut-off of 500 eV. Relatively large calculations were performed with either 3 x 3 x 3 or 4 x 4 x 4 perovskite unit cells, corresponding to 135 and 320 atoms, respectively. The calculations were carried out using the Brillouin zone sampled with a (3 x 3 x 3) or (2 x 2 x 2) Monkhorst-Pack mesh k-points grid. The lattice parameters were extracted from the equilibrium volume after a structural relaxation run during which the cell shape, cell volume, and atomic positions were relaxed. We also performed Birch-Murnaghan type calculations in which only the atomic positions were allowed to relax. The lattice parameters obtained from both approaches were almost identical (the difference being less than 0.05%), showing that the materials were not undergoing any significant phase change (see Supplemental Material).

Chemical expansion coefficients were extracted from the lattice parameters of 5 compositions, corresponding to materials with 0, 1, 2, 3 and 4 oxygen vacancies (i.e. 0, 2, 4, 6, 8 dopant cations). The dopant cations and oxygen vacancies were introduced at random in the simulation. We performed calculations on several random configurations for the same vacancy concentration and found that the lattice parameter was not influenced by different starting configurations (see Supplemental Material). Due to the relatively small changes in the lattice parameters vs. dopant concentration, we find a significant scatter in our data, which sometimes does not show a perfect Vegard-type behaviour. For this reason, we estimate an error on the calculated chemical expansion coefficients by fitting different compositional ranges and calculating the change in the chemical expansion coefficient.

Molecular Dynamics

The interaction potential used for the molecular dynamics simulations of Sr and Mg-doped $LaGaO_3$ is known as the DIPole Polarizable Ion Model (DIPPIM) and includes a pair potential (a Buckingham-like term plus Coulombic interactions), together with an account of the polarization effects that result from the induction of dipoles on the ions. A potential file is reported as Supplemental Information. The accuracy of this model was found to be similar to that of DFT calculation for several oxide materials [42–46], and the lower computational cost allows the performance of longer simulations on bigger systems. The lattice parameters for the studied systems were obtained by performing molecular dynamics simulations with 6 x 6 x 6 supercells in an NPT ensemble, at the required temperatures. We used an isotropic barostat and thermostats as described by Martyna et al [47,48] and we set the external pressure to zero. The isotropic barostat enforced a cubic perovskite symmetry. The lattice parameters were averaged over long trajectories (~ 0.1 ns). All these calculations were performed with an in-house code called PIMAIM. The DIPPIM potential has been recently implemented in the freely available CP2K code. In addition to these "realistic" potentials, we also constructed "ideal" systems in which the radius of the dopant cation was changed. This was done by manually modifying the short-range interaction parameters of the potentials, which are directly related to the cation size. This allowed us to study systems in which, for instance, the dopant cation had exactly the same radius as the host cation. This approach has been successfully used in several previous studies by authors of this paper [20,25,46,49].

Results

The origin of chemical expansion

As described in the introduction, substitution of trivalent La with divalent Sr results in the formation of charge compensating oxygen vacancies through the charge neutrality equation $[Sr'_{La}] = 2[V_O^{\cdot\cdot}]$ written in Kröger-Vink notation [9], when ionic, rather than electronic, compensation prevails. The lattice parameters of both $La_{1-x}Sr_xGaO_{3-x/2}$ (LSG) and $LaGa_xMg_{1-x}O_{3-x/2}$ (LGM) increase with increasing substitution

(x), as shown by the experimental data in Fig. 1 from Huang and Goodenough (in which the lattice was treated as cubic, though it is worth noting that more recent studies have found it to be distorted).[11,50,51] The slope of the curve shown in the figure is defined as the stoichiometric expansion coefficient, α_S, divided by 2. Such expansion vs. composition data are often found to be linear (though non-linear behavior has also been observed [13]) and can therefore be approximated by the following equation:

$$\epsilon=\frac{a-a_0}{a_0}=\alpha_S\Delta\delta=\alpha_S\frac{x}{2} \quad (1)$$

where a and a_0 are the cubic, or pseudo-cubic, final and initial lattice parameters, respectively, $\Delta\delta$ is the change in oxygen vacancy content per formula unit, and x is the divalent acceptor dopant concentration in e.g. $La_{1-x}Sr_xGaO_{3-x/2}$. Alternatively, the stoichiometric expansion coefficient can be defined by the change in oxygen vacancy concentration (in this case denoted as $\alpha_S^{[]}$), facilitating comparison across different crystal structures as discussed in the introduction and ref [30].

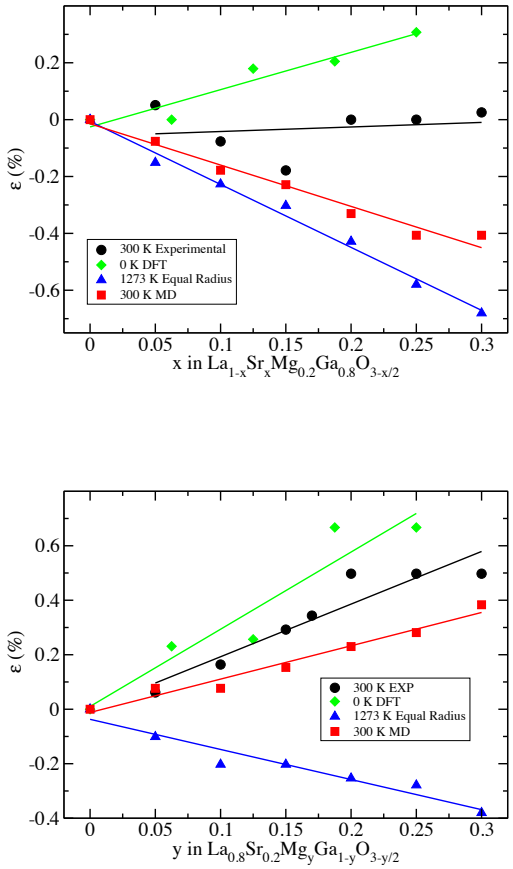

Figure 1: Chemical expansion for A-site (Sr for La) and B-site (Mg for Ga) substitution in $LaGaO_3$. Experimental data from Huang and Goodenough are reported as black circles. MD simulations at 300 K and static DFT calculations are reported as red squares and green diamonds, respectively. The results of an equal radius calculation are reported as blue triangles. Solid lines are linear fits of the data.

The coefficients of stoichiometric expansion for LSG and LGM, and other materials for comparison, are summarized in table 1. Despite having about a 6% larger ionic radius for Sr substitution of La (see table 2), α_S values for LSG and LGM are relatively small, or even negative! For example, for full substitution of La with Sr, in $La_{1-x}Sr_xGa_{0.8}Mg_{0.2}O_{2.9-x/2}$ a stoichiometric expansion of -0.32% is predicted from α_S (see Table 1 in Supplemental Material) hinting that lattice relaxations associated with the compensating oxygen vacancies play a role in contracting the lattice, as elucidated below. MD simulations at 300 K (red squares) and DFT calculations (green diamonds) are also reported in Fig. 1. For both Mg and Sr doping, DFT calculations overestimate, and MD data underestimate, the experimentally measured stoichiometric expansion. The difference from theory and experiment appears large in the figure due to the small expansions. However, there is less than a 0.6% deviation in the calculated values from the experimental lattice parameters (not shown), which is generally considered an excellent agreement [52]. In table 1 we also report an estimate of the error associated with the stoichiometric expansion coefficients calculated from DFT.

Table 1: Experimentally determined stoichiometric expansion coefficients and corresponding oxygen vacancy radii for different materials together with the DFT values obtained in this work. The chemical expansion coefficients and r_V for A-site and B-site doped $LaGaO_3$ were obtained from averaging several experimental values (which we report in the SI) taken from refs. [11,50].

Material	α_S	$\alpha_S^{[]}$ [cm^3 x 10^{24}]	r_V [Å]	Ref.
Fixed valence substitution				
$La(Ga,Mg)O_3$ (Sr A-site substitution)	0.008	0.48	1.30	[11,50]
$La_{1-x}Sr_xGa_{0.8}Mg_{0.2}O_{3-x/2}$ (DFT)	0.026 ± 0.004	1.6	1.41	This work
$(La,Sr)GaO_3$ (Mg B-site substitution)	0.056	3.3	1.29	[11,50]
$La_{0.8}Ga_{1-x}Mg_xO_{3-x/2}$ (DFT)	0.057 ± 0.008	3.4	1.30	This work
$La_{1-x}Sr_xAlO_3$	0.017	0.93	1.36	[53]
$La_{1-x}Sr_xAlO_3$ (DFT)	0.018 ± 0.014	0.98	1.38	This work
$SrTi_{1-x}Ga_xO_3$ (DFT)	0.040 ± 0.021	2.4	1.57	This work
Multivalent cation				
$CeO_{2-\delta}$*	0.10	4.0	1.16 9	[20]
$Pr_{0.1}Zr_{0.4}Ce_{0.5}O_{1.95-\delta}$*	0.046	1.7	0.96 6	[19]
$La_{0.9}Sr_{0.1}Ga_{0.95}Ni_{0.05}O_{3-\delta}$ (800-900 °C, oxidizing conditions)	0.040-0.049	2.4-2.9	1.24-1.30	[32]
$SrTi_{0.65}Fe_{0.35}O_{3-\delta}$ (700-1000 °C, oxidizing conditions)	0.040-0.049	2.38-2.92	1.38-1.43	[54]

*these compounds have the fluorite structure

In order to extract the role of relaxations around oxygen vacancies in the lattice, a substitutional cation equal-radius approach was performed (by means of Molecular Dynamics

simulations) to model the data, as done in a previous work on fluorite-structured materials.[20] In this case, the stoichiometric expansion (or contraction) is computationally predicted when the substitutional cation (i.e., Sr or Mg) radius is set equal to that of the host cation (i.e., La or Ga). This approach, in effect, isolates the role of the other defect, i.e., oxygen vacancies, introduced during substitution, on lattice relaxation. The equal-radius results are shown as blue triangles in Fig. 1. Clearly, oxygen vacancies cause the material to contract, a result previously found in fluorite oxides [20,22,36], and recently in perovskite materials [22].

Table 2: Shannon radii for the different cations and anions reported in table 1. [55] The number between parentheses represents the coordination of the ion. Where applicable, ions are assumed to adopt the high spin state.

Ion	Radius (Å)
Sr^{2+} (XII)	1.44
La^{3+} (XII)	1.36
Ce^{4+} (VIII)	0.97
Ce^{3+} (VIII)	1.143
Mg^{2+} (VI)	0.72
Ga^{3+} (VI)	0.62
Al^{3+} (VI)	0.535
Y^{3+} (VIII)	1.019
Zr^{4+} (VIII)	0.84
Ti^{4+} (VI)	0.605
Ni^{3+} (VI)	0.60
Ni^{2+} (VI)	0.69
Fe^{4+} (VI)	0.585
Fe^{3+} (VI)	0.645
O^{2-} (VI)	1.40

In Figure 2, we report DFT calculations for two other perovskite-structured materials, Sr doped $LaAlO_3$ (LSA) and Ga-doped $SrTiO_3$ (STG), along with experimental data for LSA [53]. It is worth noting that, for the latter, STG, case, only computational data from the present work are available, and, as performed for the previous materials studied here (LSG and LGM), the acceptor dopants (Sr in LSA and Ga in STG) are restricted to be charge compensated for by oxygen vacancies, as opposed to holes. Experimentally in LSA (as for LSG or LGM), the acceptor will be partially compensated for by holes (to a small degree), rather than oxygen vacancies [56,57], leading to a slight underestimation of α_S by the computational approach, in which more oxygen vacancies are generated per dopant. The stoichiometric expansion coefficients, extracted from the slopes, are reported in Table 1. As in the LSG and LGM cases above, the lattice expansion, even for large amounts of dopants, is small. As before, the scatter in the points shown in Figure 2 likely arises from the small range of expansion.

A key advantage of simulations is their ability to provide atomistic level visualization of lattice relaxations around defects. As shown in Fig. 3, oxide ions relax towards a $V_{\ddot{O}}$ leading to a contraction in the LSA system. LSG, which exhibits more complicated relaxations (though similar to the LSA case) due to a less symmetric perovskite structure compared to LSA [58], is shown in the Supplementary Information together with STG. In the figure, the grey arrows show displacements that are greater than 0.15 Å with a pattern of displacements that is reminiscent of that observed in fluorite oxides.[20,25] All the 8 oxide ions that are nearest neighbor to the vacancy move towards it. This leads to a significant tilting of the AlO_6 octahedra, which in turn displaces some of the next nearest neighbor oxide ions (indicated by red circles) away from the vacancy. On the other hand, the 4 cations that are nearest neighbor to the vacancy are displaced away from it (these displacements are of the order of 0.12 Å and therefore not shown by the arrows). Overall, it is clear that the magnitude of these distortions results in a net contraction of the lattice, which explains the equal-radius results of Figure 1. (It is noted that the magnitude of this net contractive effect, and the corresponding oxygen vacancy radius discussed later, were determined from a series of simulations, in many cases where the vacancy and dopant were not nearest-neighbor.) As with the fluorite structure, it is not only these contractions around the oxygen vacancy, but also the cation radii changes that drive stoichiometric expansion. In the next section of this paper, an analytical model for stoichiometric expansion in cubic perovskite materials is developed and applied to the available experimental and computational data on these materials.

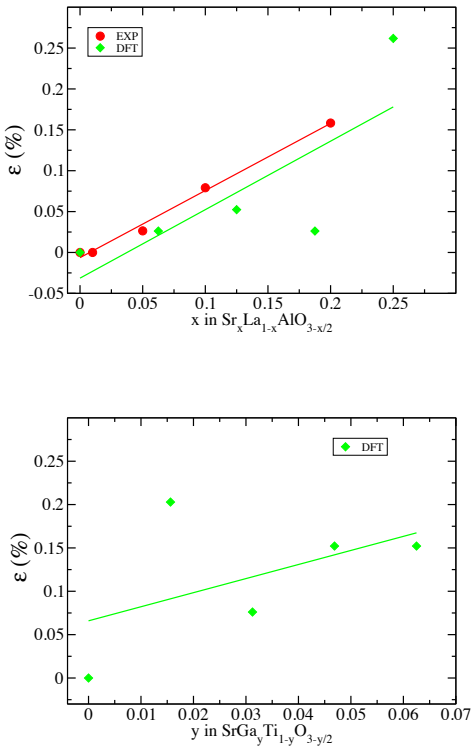

Figure 2: Percentage chemical expansion for A-site (Sr for La) and B-site (Ga for Ti) substitution in $LaAlO_3$ and $SrTiO_3$, respectively. Experimental data are reported as red circles. [53]

A model for stoichiometric expansion in perovskites oxides

As discussed above, two factors are primarily responsible for stoichiometric expansion in the materials studied here: the change in lattice parameter associated with substitution of differently sized cations and the relaxation around oxygen vacancies. Several predictive models of perovskite lattice parameters exist based on microscopic parameters (such as ionic radii, tolerance factors, valence electrons and electronegativity) [22,59–63], with one model including the role of oxygen vacancies [22]. However, some models are over-parameterized [59] while others use incorrect coordination numbers for the cations [61]. Also, some of these models [60], while in principle correct, lead to very complicated equations for α_S, which can only be solved numerically. Lastly, the model considering oxygen vacancies [22] does not take into account the fact that the lattice parameter is more responsive to B-site rather than A-site substitution, which has been observed experimentally [22,59–62] and is also discussed below. For this reason, we have decided to develop our own model, which is a modified version of that introduced by Jiang et al. [61].

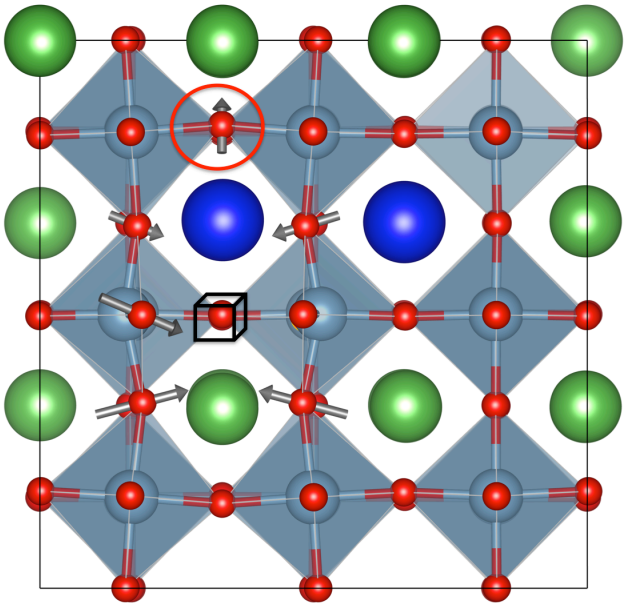

Figure 3: Lattice relaxation around an oxygen vacancy (black cube) in $LaAlO_{3-\delta}$ from DFT simulations. Green, dark blue, light blue and red spheres are La, Sr, Ti and O ions, respectively. We note that, for the sake of clarity, the sizes of the sphere radii in this figure are not always proportional to the sizes of the ionic radii

In the present model, the lattice parameter of a perovskite material is a combination of the A-O and B-O bond distances, where A (B) is the big (small) 12-fold (6-fold) coordinated cation. In a perfectly cubic perovskite system, the lattice parameter can be written as:

$$a = 2(r_B + r_X) \text{ or } a = \sqrt{2}(r_A + r_X) \quad (2)$$

where r_A, r_B, and r_X are the average ionic radii for the A-site, B-site, and anion site, respectively. Clearly, the above equation provides two solutions to the lattice parameter, each of which will likely be different. Therefore, the following equation, which weights the impact of the A and B site radii with empirical parameters (*A, B*, and *C*) is introduced.

$$a = \frac{A}{\sqrt{2}}(r_A + r_X) + B(r_B + r_X) + C \quad (3)$$

The empirical parameters, reported in table 3, were derived by fitting a set of 77 experimental lattice parameters for stoichiometric perovskite oxides previously gathered from the existing literature by Jiang *et al* [61]. We note that we fitted all three parameters simultaneously in a multivariable fit performed with Gnuplot, while in previous works these parameters had been derived from two independent fits [60,61]. (Note also that our previously reported values for A and B in ref. [32] were a result of the preliminary two-stage fitting, whereas the values in the present work are considered more accurate.) It is noted here that this method for predicting lattice parameters is derived from stoichiometric materials (as was also done for the derivation of ionic radii by Shannon).[55] In this work we, as we and others have done in the past, are extending these models to defective oxides, and in the process introducing an empirical parameter, the oxygen vacancy radius.

Our model predicts the experimental lattice parameters with an average error of 0.83% (see also figure in Supplemental Material), slightly better than the 0.89 % obtained from Jiang's model [61] and a significant improvement over the Moreira's model (1.82%) [60]. We also point out that B > A, which indicates that the lattice parameter is significantly (by almost a factor of 2!) more sensitive to changes in the B cation than the A cation, as can be easily observed by previous studies of the effects of isovalent doping (e.g. $SrTiO_3$ vs. $BaTiO_3$ and $SrTiO_3$ vs. $SrFeO_3$) [61].

Table 3: Empirical parameters used in equation 3.

A	*B*	*C*
0.816	1.437	-0.609

By substituting equation (3) into equation (1), an expression for α_S is derived. As discussed below, α_S is further broken down into components relating the expansion of the lattice to changes in radii of the cations and relaxation around oxygen vacancies. The former are estimated from published ionic radii [55] and the latter are fitted with the aid of the empirical parameters in table 3. The details of the derivation are reported in the appendix; below is a summary. In order to express the stoichiometric expansion of a perovskite upon changes in composition, one may write the chemical formula as:

$$A_x^{sub} A_{1-x}^{host} B_y^{sub} B_{1-y}^{host} O_{3-\delta} \quad (4)$$

For the aforementioned case of acceptor doping of $LaGaO_3$, e.g., its chemical formula is written as:

$$Sr_x La_{1-x} Mg_y Ga_{1-y} O_{3-(x+y)/2} \quad (5)$$

Similarly, to describe chemical expansion that involves reduction of a B-site cation, when multiple cations are present on the B-site (as is typically observed in SOFC perovskite cathodes, and as has been recently applied to Sr- and Ni-doped $LaGaO_3$ [32]), the chemical formula is written as:

$$Sr_x^{2+} La_{1-x}^{3+} (Ga_{1-z}^{3+} Ni_z^{2+})_y (Ga_{1-z}^{3+} Ni_z^{3+})_{1-y} O_{3-\frac{x+yz}{2}} \quad (6)$$

. The stoichiometric expansion in both cases is expressed as:

$$\epsilon = \frac{a-a_0}{a_0} = \alpha_A(x-x_0) + \alpha_B(y-y_0) + \alpha_V\frac{(x-x_0+(y-y_0)z)}{2} \quad (7)$$

where the constant z represents the fraction of the B sublattice initially available for substitution. For the case of LSGM in equation 5, z is equal to 1 (this is why that constant does not appear in equation 5). Equation 7 contains three coefficients of expansion terms, which are proportional to the changes in A-site cation radius (α_A), B-site cation radius (α_B), and anion radius (α_V). Here 6-fold coordinated oxygen is used, in agreement with Shannon's treatment for perovskites [55], though it is noted that O has also been considered as 2-fold coordinated due to the distorted octahedron [59]. Following the derivation reported in the appendix, making use of the equality of equation 7 with the derived expansion from equation 3, mathematical expressions for the three expansion coefficient terms can be obtained and are reported in Table 4.

Table 4: Mathematical expressions for the chemical expansion coefficients used in equation (7). $r_{A^{host}}$ and $r_{B^{host}}$ are the A-site and B-site host cation radii, while $r_{A^{sub}}$ and $r_{B^{sub}}$ are the radii of the substitutional cations. Finally, r_V is the oxygen vacancy radius, which is obtained from the expression for α_V.

Term	Mathematical Expression
α_A	$\frac{A}{\sqrt{2}}\frac{r_{A^{sub}} - r_{A^{host}}}{a_0}$
α_B	$B\frac{r_{B^{sub}} - r_{B^{host}}}{a_0}$
α_V	$\frac{1}{3}(\frac{A}{\sqrt{2}} + B)\frac{(r_V - r_O)}{a_0}$
r_V	$r_V = \frac{3\alpha_V a_0}{\left(\frac{A}{\sqrt{2}} + B\right)} + r_O$
α_S	$\alpha_V + 2\alpha_A$ for A-site substitution $\alpha_V + \frac{2}{z}\alpha_B$ for B-site substitution

The only unknown parameter in Table 4 needed to predict expansion coefficients is $\boldsymbol{r_V}$. For the particular case where z is equal to 1 and for only A site doping, equation (7) becomes:

$$\frac{a-a_0}{a_0} = (x-x_0)\left(\alpha_A + \frac{\alpha_V}{2}\right) \quad (8)$$

If the lattice expansion, $\frac{a-a_0}{a_0}$, is plotted vs. the change in A-site dopant concentration, $(x-x_0)$, the slope is equivalent to $\alpha_S/2$ using the relevant expression for α_S in table 4. A similar expression relates α_S to α_B and α_V for B-site doping. Since α_A and α_B can be determined from known ionic radii, one can derive α_V, and hence, r_V from these relationships. By this approach, the data in Table 1 (α_S) were used to estimate r_V for these materials as also reported in table 1. For $LaGaO_3$ experimental data, we obtain an average r_V of 1.30 Å and 1.29 Å for A-site and B-site doping, respectively. In both cases, r_V is smaller than the radius of an oxide ion in the perovskite structure, equal to 1.40 Å. This result confirms our previous observation (see Figures 1-3) that oxygen vacancies lead to a contraction of the lattice parameter. However, some of the other materials in Table 1 exhibit a vacancy radius similar to or even greater than the oxide ion radius. The vacancy radii extracted from the DFT calculations are in reasonably good agreement with those derived from the experimental data, though for A-site doping we obtain values that are slightly larger than the radius of oxygen. This is a consequence of the overestimate of the chemical expansion coefficient from DFT, reported in Table 1.

Similarly oxygen vacancy radii are determined for materials exhibiting stoichiometric expansion upon reduction of a multivalent cation. Here, we limit the discussion to those multivalent cations that are expected to show ionic/polaronic behavior, as described in their respective cited papers. For $La_{0.9}Sr_{0.1}Ga_{0.95}Ni_{0.05}O_{3-\delta}$, which changes oxygen stoichiometry in response to a valence change of Ni, the oxygen vacancy radius is calculated to be 1.24-1.30 Å at 800-900 °C, which is similar to the theoretically-derived value for B-site doping of $LaGaO_3$ given above. However, for $SrTi_{0.65}Fe_{0.35}O_{3-\delta}$, the oxygen vacancy radius (1.38-1.43 Å at 700-1000 °C) is found to be almost identical to the oxide ion radius. We note that in all cases, the values obtained here are either similar to or larger than the vacancy radii calculated for fluorite-structured materials, which is in agreement with the recent study by Chatzichristodoulou et al. [22]

Discussion

Having noted the generally smaller α_S for perovskites vs. fluorites, we investigated the process of perovskite chemical expansion through 1) performing atomistic simulations of local relaxations and overall expansion/contraction during changes in composition, and 2) deriving an empirical model relating stoichiometric expansion coefficients and ionic radii, including effective oxygen vacancy radii. In this section we turn to interpreting the results and discussing the limits of their applicability.

Origin of lower chemical expansion in perovskite oxides as compared to fluorite oxides

One of the motivations of this paper was to understand the observation by Atkinson and Ramos that chemical expansion in perovskite materials is significantly smaller than in fluorites. Indeed, this point can be observed in Table 1, where both α_S and α_S[] are often found to be smaller in perovskites. Our results can be used to shed some light on this observation. Looking at the vacancy radii reported in Table 1, one sees that these are larger than the values obtained for fluorites, which implies that the lattice contracts less around the vacancy in the perovskite structure. This result implies that the origin of the smaller chemical expansion observed in perovskite materials cannot be explained in terms of a larger contraction around the oxygen vacancy. A closer inspection of Table 1 provides an alternative, simpler explanation. Indeed, in many cases the low chemical expansion coefficient occurs simply because the dopant cation has a radius that is close to that of the host, e.g. Sr (1.44 Å) and La (1.36 Å). In this case, the lower chemical expansion coefficient is largely caused by a small α_A rather than by a large (and negative) α_V. In the opposite case, when the dopant cation

is significantly larger than the host (e.g. Mg is 16% bigger than Ga, similar to the 18% increase in Ce radius change upon reduction), $\alpha_S^{[]}$ is actually quite large (3.3 x 10^{24} cm^3 for $LaGaO_3$ with Mg B-site substitution) and comparable to those observed in fluorite materials (4.0 x 10^{24} cm^3 for $CeO_{2-\delta}$ reduction) (see Table 1). Finally, we note that in the work of Atkinson and Ramos discussed in the introduction, the comparison between fluorite and perovskite oxide stoichiometric expansions were based primarily on α_S (and not $\alpha_S^{[]}$) of reduction of chromite compounds with and without transition metal doping. The different units for stoichiometric expansion, the possibility for charge delocalization with transition metals, and the small change in Cr radius likely explain a large part of their observed differences.[21,30,32,33,55]

Discussion of Empirical Model

In this work we have introduced a new model for the lattice parameter in perovskites (see equation 3), which we find possesses a series of desirable features. Indeed, despite its simplicity and relatively small number of parameters, equation 3 predicts the lattice parameters of stoichiometric perovskites with a higher accuracy than the models by Jiang [61], Moreira [60] and Chatzichristodoulou [22]. Predicting lattice parameters of stoichiometric perovskites is an important result, and we hope that equation 3 will be used for this purpose in future work.

A second important point is the use of our model to extract vacancy radii for a variety of perovskites. We note that Chatzichristodoulou et al. also used a similar approach and that their model is actually similar to ours; only the coefficients equivalent to A, B, and C are very different (i.e., A ~ B ~1, C = 0) [22]. This difference, however, has important consequences. Indeed, their model does not take into account that the lattice parameter of perovskite materials is significantly more sensitive to changes in the B cation than the A cation, which has been observed experimentally [61]. This difference is probably a consequence of the limited data-set used to fit their parameters (they only used data for $LaGaO_3$); incidentally, this also explains why their model yields a relatively high error (1.28%) when used to predict the lattice parameters of other stoichiometric perovskites.

Finally, on a more technical point, we note the importance of fitting all three parameters of equations (3) simultaneously in a multivariable fit, rather than in a 2-step fit, as done in refs [60,61]. Indeed, when a 2-step fitting procedure is used, one obtains a model that is not as good at predicting the lattice parameter of stoichiometric perovskite compounds (average error of 1.41%) than the model obtained from a multivariable fit (0.82% average error). Also, the r_V values can differ significantly, see for instance Table 1 in this paper and Table 2 in ref. [32] (where a 2-step fitting was used), for $La_{0.9}Sr_{0.1}Ga_{0.95}Ni_{0.05}O_{3-\delta}$, showing that the vacancy radius changes by as much as 20%.

Trends in rV

In table 1, r_v varies from 1.24 Å to 1.57 Å for the perovskite materials, equal to ~27% variation. Similarly, r_v changes from 0.99 Å to 1.17 Å for the fluorite oxides, with lattice parameters smaller than that of ceria exhibiting smaller r_V as noted previously [22,25]. Considering only fixed valent doping, a slight decrease in r_V for the perovskites with increasing lattice parameter is found for the data in table 1, however, when considering the multivalent and computational data, the variation in values makes it difficult to conclusively find a trend. One reason why a trend may not be evident is that the change in lattice parameter for the studied perovskites here is narrower (about 3.4%) as compared to the fluorite case (5.7%) [25].

In principle, the vacancy radius may also be influenced by the magnitude of the expansion of the cations. It is worth reiterating that, in the model, r_V is related to all lattice relaxations not accounted for by the inputted cation radius change. This is dominated by relaxations around oxygen vacancies (as shown by the DFT calculations in Figure 3), but may also include small effects from distortions around cations. Figure 4 shows that r_V tends to decrease for substitution with larger cations, though, if greatest weight is placed on the experimental data, the trend is the smallest. For the largest lattice mismatch, i.e., largest cation radius change, one would expect lattice relaxations, not accounted for by the simple hard sphere type model, around cations to be the greatest (i.e., a smaller r_v). This result highlights that for larger cation radii changes, r_V may be more sensitive to lattice relaxations additional to the contraction around oxygen vacancies. Lastly, as discussed in the next section, Frade et al. described an increasing trend in stoichiometric expansion coefficient as the lattice approached a tolerance factor of unity (i.e., ideal cubic symmetry) [64]. In the present case, a plot of r_V against tolerance factor (calculated based on the initial acceptor dopant and vacancy content) did not reveal a trend, which may result from a more limited data set here.

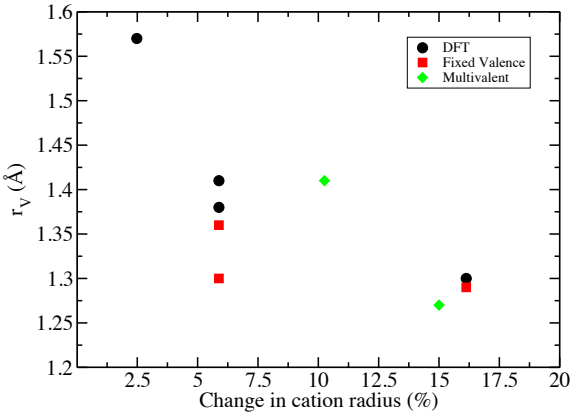

Figure 4: Vacancy radii from table 1 compared to percent change in cation radius. r_v values for multivalent cation radii change are averages from table 1.

Limits of Applicability

As noted in the introduction, the treatment in this work has largely been limited to perovskites with near-cubic symmetry, ionic cations with localized charge, non-magnetic cations, and no appreciable ordering or defect association. Furthermore, the Shannon ionic radii and DFT calculations are valid at low temperatures. In practical device operating conditions and commonly used compositions, many of these neglected factors may also influence chemical expansion behavior. For example, in perovskites, a very strong influence of temperature on chemical expansion coefficients, e.g., increasing α_S by 20% over just a 100-300 °C range, has been observed in some cases [32,33,54,57,65], although the exact reason (e.g., order-disorder transitions, symmetry changes, or bond strength effects) remains under investigation. In other perovskite systems no temperature effect was observed [17]. Ideally future work to understand perovskite chemical expansion behavior would seek to isolate the impact of each of these factors to understand which are dominant. On the other hand, many of these properties (e.g., temperature, spin state, and symmetry or charge localization and symmetry) are coupled in such a way that it becomes a complex challenge to attribute chemical expansion behavior to any one factor..

Conclusions

The origin of stoichiometric expansion in perovskite oxides was explored using both empirical modeling of experimental and computational data and atomistic simulations. An empirical model, based on previous approaches in the literature, was developed to predict the lattice constant of perovskite oxides. The model indicated that the lattice constant is more sensitive to changes of the B site cation radius as compared to the A site cation radius, as previously observed [60,61]. A mathematical expression was formulated to describe the relaxations in the lattice due primarily to oxygen vacancies, resulting in the derivation of the radius of an oxygen vacancy, r_V. Additionally, computational results were used to visualize the relaxations around the vacancy. In most cases, r_V was found to be smaller than the radius of an oxide ion, in agreement with prior studies, though r_V was larger for the perovskites than for previously studied fluorites. As a result, the generally larger stoichiometric expansion coefficients found in fluorites could not be explained by the difference in r_V. Instead, the difference is mostly attributed to larger changes in the cation radii in fluorite oxides as compared to typical dopants/multivalent cation radii changes in perovskites and to the different units of the stoichiometric expansion coefficient used in previous studies [30]. Trends of r_V with lattice parameter, tolerance factor, and cation radius changes were examined. The limitations of the present model and an overview of other factors contributing to chemical expansion were also discussed.

Appendix: Derivation of Equations Relating Chemical Expansion to Ionic Radii

This derivation applies to 3-3 or 2-4 perovskites with general formula:

$$A_x^{sub}A_{1-x}^{host}B_y^{sub}B_{1-y}^{host}O_{3-\delta} \quad \text{(A1a)}$$

e.g.,

$$La_{1-x}^{3+}Sr_x^{2+}(Ga_{1-z}^{3+}Ni_z^{2+})_y(Ga_{1-z}^{3+}Ni_z^{3+})_{1-y}O_{3-\frac{x+yz}{2}} \quad \text{(A1b)}$$

$$Sr_{1-x}^{2+}M_x^{1+}(Ti_{1-z}^{4+}Fe_z^{3+})_y(Ti_{1-z}^{4+}Fe_z^{4+})_{1-y}O_{3-\frac{x+yz}{2}} \quad \text{(A1c)}$$

$$Sr_xLa_{1-x}Mg_yGa_{1-y}O_{3-(x+y)/2} \quad \text{(A1d)}$$

In these formulae, x and y represent *variable* fractional amounts of *substitution* on A and B sites, respectively, relative to the host lattice, contributing to chemical expansion. In some cases, such as when two types of cations are already present on the B site of the *host* lattice, only a portion of that sublattice may be available for substitution; this fraction is described by the *fixed* constant z (see eq. A1b and A1c). Three potential processes leading to chemical expansion are therefore described here: substitution of a new cation on the A site, substitution of a new cation on the B site, and reduction of an existing multivalent cation partially occupying the B site. This latter possibility is considered in the description of the B site in equations A1b and A1c. In those cases, the "substitutional cation" is a mixture of a fixed valent and reduced multivalent cation and the "host cation" is a mixture of the same fixed valent cation and the oxidized multivalent cation. Equation A1d represents the other two simpler cases of fixed valent acceptor substitutions on the A and/or B sites. (Note, in the simpler case of eq. A1d, the value of z, which appears in eqs. A1b and A1c, can be considered 1.)

As shown in the article, the chemical expansion (eq. A2) can be described as three terms, one relating to the expansion originating from changes in the A-site cation(s), one relating to changes in the B-site cation(s), and one expressing expansion originating from changes on the anion site. Each term is proportional to the amount (per formula unit) of substitution taking place on the corresponding lattice site, as defined by the chemical formulas. Recall that a is the pseudo-cubic lattice parameter. a_0, x_0, and y_0 represent the initial condition, while a, x, and y represent the final condition after expansion. Note that the oxygen stoichiometry change depends on the valence states of the host and substitutional cations in this model.

$$\epsilon = \frac{a-a_0}{a_0} = \alpha_A(x-x_0) + \alpha_B(y-y_0) + \alpha_V\frac{(x-x_0+(y-y_0)z)}{2} \quad \text{(A2)}$$

As described in the article, the lattice parameter in perovskite oxides can be described empirically using the following formula, in an approach similar to that of Jiang *et al* [61].

$$a = \frac{A}{\sqrt{2}}(r_A + r_X) + B(r_B + r_X) + C \quad \text{(A3)}$$

where A, B, and C are empirical fitting constants determined in this work, as described in the supplemental material, and r_A, r_B, and r_X are the average of radius for A site cation, B site cation, and oxide ion/oxygen vacancy, respectively. Substituting eq. A3 into eq. A2:

$$\alpha_A(x-x_0)+\alpha_B(y-y_0)+\alpha_V\frac{(x-x_0+(y-y_0)z)}{2}=\frac{\frac{A}{\sqrt{2}}(r_A-r_A^0+r_X-r_X^0)+B(r_B-r_B^0+r_X-r_X^0)}{a_0} \quad \text{(A4)}$$

For the specific case when only the B-site cation undergoes reduction/oxidation/substitution (i.e. change in y but not x):

$$x-x_0=0 \quad \text{(A5a)}$$

$$r_A-r_A^0=0 \quad \text{(A5b)}$$

Equation A4 simplifies to:

$$(y-y_0)(\alpha_B+\alpha_V\tfrac{z}{2})=\frac{\frac{A}{\sqrt{2}}(r_X-r_X^0)+B(r_B-r_B^0+r_X-r_X^0)}{a_0} \quad \text{(A6)}$$

In the special case where there is no change in radius on the B-site during substitution (i.e., equal radius approximation), $r_B = r_B^0$, and $\alpha_B = 0$, which results in further simplification of equation A6 and, as discussed below, provides an equation to estimate the effective radius of an oxygen vacancy, provided α_V is known:

$$(y-y_0)(\alpha_V\tfrac{z}{2})=\frac{(\frac{A}{\sqrt{2}}+B)(r_X-r_X^0)}{a_0} \quad \text{(A7)}$$

Next we need to define r_X and r_X^0. The anion site is occupied by oxide ions and oxygen vacancies. The oxygen concentration per formula unit is changing from 3-(x_0+y_0z)/2 to 3-(x+yz)/2, with the remainder of the 3 sites occupied by oxygen vacancies. So:

$$r_X^0=\tfrac{1}{3}\left[\left(3-\tfrac{x_0+y_0z}{2}\right)r_O+\left(\tfrac{x_0+y_0z}{2}\right)r_V\right] \quad \text{(A8)}$$

$$r_X=\tfrac{1}{3}\left[\left(3-\tfrac{x+yz}{2}\right)r_O+\left(\tfrac{x+yz}{2}\right)r_V\right] \quad \text{(A9)}$$

$$r_X-r_X^0=\left(\tfrac{x-x_0+(y-y_0)z}{6}\right)(r_V-r_O) \quad \text{(A10)}$$

As mentioned above, x-x_0 is zero for this case where we are not changing the A cation site occupancy, so equation A10 simplifies to:

$$r_X-r_X^0=\left(\tfrac{(y-y_0)z}{6}\right)(r_V-r_O) \quad \text{(A11)}$$

Substituting eq. A11 into eq. 7 gives:

$$\alpha_V=\frac{\left(\frac{A}{\sqrt{2}}+B\right)(r_V-r_O)}{3a_0} \quad \text{(A12)}$$

Re-arranging eq. A12 gives the solution for the effective oxygen vacancy radius below:

$$r_V=\frac{3\alpha_V a_0}{\left(\frac{A}{\sqrt{2}}+B\right)}+r_O \quad \text{(A13)}$$

If we want to determine r_V from the measured chemical expansion coefficient, α_S we need an expression for α_V in terms of α_S. This expression can be generated from eq. A2, still with $x = x_0$ for B-site substitution only:

$$\alpha_S\cdot\Delta\delta=\epsilon=\frac{a-a_0}{a_0}=\left(\alpha_B+\alpha_V\frac{z}{2}\right)(y-y_0) \quad \text{(A14)}$$

The change in oxygen stoichiometry ($\Delta\delta$) is given as (again noting $x = x_0$ for only B-site substitution):

$$\delta-\delta_0=\tfrac{x+yz}{2}-\tfrac{x_0+y_0z}{2}=(y-y_0)\left(\tfrac{z}{2}\right) \quad \text{(A15)}$$

Using equation A15, equation A14 becomes:

$$\alpha_S\left(\tfrac{z}{2}\right)=\left(\alpha_B+\alpha_V\tfrac{z}{2}\right) \quad \text{(A16)}$$

which is rearranged as follows:

$$\alpha_V=\alpha_S-\frac{2\alpha_B}{z} \quad \text{(A17)}$$

Since α_S is measured experimentally (or determined by theoretical calculations of lattice parameter changes upon changes in oxygen content), only an expression for α_B is needed to derive α_V. Therefore, in order to isolate α_B in eq. A6, r_X is set to be equivalent to r_X^0, thus $\alpha_V = 0$. In this case (still for B-site substitution, so also $r_A = r_A^0$ and $x = x_0$), eq. A6 simplifies to:

$$\alpha_B=\frac{B(r_B-r_B^0)}{a_0(y-y_0)} \quad \text{(A18)}$$

Here, we need an expression for the change in average B-site radius, r_B-r_B^0 between the final occupancy $B_y^{sub}B_{1-y}^{host}$ and initial occupancy $B_{y_0}^{sub}B_{1-y_0}^{host}$.

$$r_B-r_B^0=\left[yr_{B^{sub}}+(1-y)r_{B^{host}}\right]-\left[y_0r_{B^{sub}}+(1-y_0)r_{B^{host}}\right] \quad \text{(A19)}$$

Equation A19 simplifies to:

$$\frac{r_B-r_B^0}{y-y_0}=r_{B^{sub}}-r_{B^{host}} \quad \text{(A20)}$$

Note that for the case of multiple cations occupying the B-site (as in eq. A1b) these substitutional and host B-cation radii are averages. An example of calculating these values, using the formula in eq. A1b, is given below:

$$\begin{aligned}r_{B^{sub}}-r_{B^{host}}&=[(1-z)r_{Ga^{3+}}+zr_{Ni^{2+}}](y-y_0)\\&\quad+[(1-z)r_{Ga^{3+}}+zr_{Ni^{3+}}]\big((1-y)-(1-y_0)\big)\\&=z(r_{Ni^{2+}}-r_{Ni^{3+}})\end{aligned} \quad \text{(A21)}$$

Equation A20 can be substituted into equation A18, yielding the final expression for α_B, which is useful for estimating α_B for known B-site cation radii:

$$\alpha_B=\frac{B}{a_0}\left(r_{B^{sub}}-r_{B^{host}}\right) \quad \text{(A22)}$$

Then eqs. A22, A17, and A13 may be used to determine the oxygen vacancy radius for the case of B-site substitution. It is noted that $r_{B^{sub}}$ and $r_{B^{host}}$ depend on z (see, e.g., eq. A21), so that the appearance of z in equation A17 is not unexpected.

Now we move to consider the case of changes in the A-site cation, but not in the B-site cation, to derive equations that enable a calculation of the oxygen vacancy radius in this case,

following the same approach as above. For A-site substitution only, y-$y_0 = 0$. Then equation A2 simplifies to:

$$\alpha_S \cdot \Delta\delta = \epsilon = \frac{a-a_0}{a_0} = \left(\alpha_A + \frac{\alpha_V}{2}\right)(x - x_0) \quad \text{(A23)}$$

In this case the change in oxygen non-stoichiometry is:

$$\delta - \delta_0 = \frac{x+yz}{2} - \frac{x_0+y_0 z}{2} = (x - x_0)\left(\frac{1}{2}\right) \quad \text{(A24)}$$

So equation A23 simplifies to:

$$\alpha_V = \alpha_S - 2\alpha_A \quad \text{(A25)}$$

Then we need an expression for α_A. Again we can say that when $r_X = r_X^0$, $\alpha_V = 0$. Combined with y-$y_0 = 0$ and $r_B = r_B^0$ for A-site substitution only, eq. A5 simplifies to:

$$\alpha_A = \frac{\frac{A}{\sqrt{2}}(r_A - r_A^0)}{a_0(x - x_0)} \quad \text{(A26)}$$

As before, we can write an expression for r_A-r_A^0 in terms of the host and substitutional radii,

$$r_A - r_A^0 = \left[x r_{A^{sub}} + (1-x) r_{A^{host}}\right] - \left[x_0 r_{A^{sub}} + (1-x_0) r_{A^{host}}\right] \quad \text{(A27)}$$

which, simplified, gives:

$$\frac{r_A - r_A^0}{x - x_0} = r_{A^{sub}} - r_{A^{host}} \quad \text{(A28)}$$

Substituting eq. A28 into eq. A26 yields the equation for α_A:

$$\alpha_A = \frac{A}{\sqrt{2}} \frac{\left(r_{A^{sub}} - r_{A^{host}}\right)}{a_0} \quad \text{(A29)}$$

Then eq. A29 can be combined with eq. A25 and the measured chemical expansion coefficient to determine α_V. Finally we need to derive the expression for oxygen vacancy radius from α_V for this case of A-site substitution only. Here again we can say that when $r_A = r_A^0$, $\alpha_A = 0$. In combination with y-$y_0 = 0$ and $r_B = r_B^0$ for A-site substitution only, eq. A4 simplifies to:

$$\alpha_V \frac{(x - x_0)}{2} = \frac{\left(\frac{A}{\sqrt{2}} + B\right)(r_X - r_X^0)}{a_0} \quad \text{(A30)}$$

Also for A-site substitution eq. 10 simplifies to:

$$r_X - r_X^0 = \left(\frac{x - x_0}{6}\right)(r_V - r_O) \quad \text{(A31)}$$

Substituting eq. A31 into eq. A30 yields:

$$\alpha_V = \frac{\left(\frac{A}{\sqrt{2}} + B\right)(r_V - r_O)}{3a_0} \quad \text{(A32)}$$

Eq. A32 is identical to eq. A12, so in the same way r_V is expressed as in eq. A13.

Then the oxygen vacancy radius for the case of A-site substitution only can be found from equations A13, A29, and A25.

Acknowledgements

The authors gratefully acknowledge the support from DOE Basic Energy Sciences, Grant number DE-SC0002633. This work used the Extreme Science and Engineering Discovery Environment (XSEDE), which is supported by National Science Foundation grant number TG-DMR110004. This research used resources of the National Energy Research Scientific Computing Center, a DOE Office of Science User Facility supported by the Office of Science of the U.S. Department of Energy under Contract No. DE-AC02-05CH11231. NHP acknowledges partial support from WPI-I2CNER, supported by the World Premier International Research Initiative (WPI), MEXT, Japan and from JSPS KAKENHI grant number 25820334. SRB and NHP thank the Progress 100 program of Kyushu University, supported by MEXT, Japan.

Notes and references

[a] Department of Nuclear Science and Engineering, MIT, Cambridge, USA
[b] School of Chemistry, Trinity College Dublin, Dublin 2, Ireland
[c] Department of Materials Science and Engineering, MIT, Cambridge, USA
[c] International Institute for Carbon Neutral Energy Research (I^{2}CNER), Kyushu University, Nishi-ku Fukuoka, Japan
† These authors contributed equally to this work
* To whom any correspondence should be addressed

Electronic Supplementary Information (ESI) available: Supplemental Figures showing ionic relaxations in $LaGaO_3$ and $SrTiO_3$, accuracy of equation (3) and chemical expansion coefficients of $LaGaO_3$. See DOI: 10.1039/b000000x/

1 *H. J. Snaith, J. Phys. Chem. Lett., 2013, **4**, 3623–3630.*
2 *S. W. Tao, J. T. S. Irvine and J. A. Kilner, Adv. Mater., 2005, **17**, 1734–1737.*
3 *G. Tsekouras, D. Neagu and J. T. S. Irvine, Energy Environ. Sci., 2013, **6**, 256.*
4 *R. Waser, R. Dittmann, G. Staikov and K. Szot, Adv. Mater., 2009, **21**, 2632–2663.*
5 *K. Szot, R. Dittmann, W. Speier and R. Waser, Phys. Status Solidi RRL – Rapid Res. Lett., 2007, **1**, R86–R88.*
6 *K. Szot, W. Speier, G. Bihlmayer and R. Waser, Nat. Mater., 2006, **5**, 312–320.*
7 *Y. Nishihata, J. Mizuki, T. Akao, H. Tanaka, M. Uenishi, M. Kimura, T. Okamoto and N. Hamada, Nature, 2002, **418**, 164–167.*
8 *H. Tanaka, M. Uenishi, M. Taniguchi, I. Tan, K. Narita, M. Kimura, K. Kaneko, Y. Nishihata and J. Mizuki, Catal. Today, 2006, **117**, 321–328.*
9 *H. L. Tuller and S. R. Bishop, Annu. Rev. Mater. Res., 2011, **41**, 369–398.*
10 *J. B. Goodenough, Annu. Rev. Mater. Res., 2003, **33**, 91–128.*
11 *K. Huang, R. S. Tichy and J. B. Goodenough, J. Am. Ceram. Soc., 1998, **81**, 2565–2575.*
12 *K. Huang, R. S. Tichy and J. B. Goodenough, J. Am. Ceram. Soc., 1998, **81**, 2576–2580.*

13 S. R. Bishop, D. Marrocchelli, C. Chatzichristodoulou, N. H. Perry, M. B. Mogensen, H. L. Tuller and E. D. Wachsman, Annu. Rev. Mater. Res., 2014, **44**.
14 B. W. Sheldon, S. Mandowara and J. Rankin, Solid State Ion., 2013, **233**, 38–46.
15 A. Atkinson and T. Ramos, Solid State Ion., 2000, **129**, 259–269.
16 S. B. Adler, J. Am. Ceram. Soc., 2001, **84**, 2117–2119.
17 S. R. Bishop, K. L. Duncan and E. D. Wachsman, J. Am. Ceram. Soc., 2010, **93**, 4115–4121.
18 S. R. Bishop, Acta Mech. Sin., 2013, **29**, 312–317.
19 S. R. Bishop, D. Marrocchelli, W. Fang, K. Amezawa, K. Yashiro and G. W. Watson, Energy Environ. Sci., 2013, **6**, 1142.
20 D. Marrocchelli, S. R. Bishop, H. L. Tuller and B. Yildiz, Adv. Funct. Mater., 2012, **22**, 1958–1965.
21 D. Marrocchelli, S. R. Bishop, H. L. Tuller, G. W. Watson and B. Yildiz, Phys. Chem. Chem. Phys., 2012, **14**, 12070.
22 C. Chatzichristodoulou, P. Norby, P. V. Hendriksen and M. B. Mogensen, J. Electroceramics, 2014, 1–8.
23 S. Omar and J. C. Nino, Acta Mater., 2013, **61**, 5406–5413.
24 D. Er, J. Li, M. Cargnello, P. Fornasiero, R. J. Gorte and V. B. Shenoy, J. Electrochem. Soc., 2014, **161**, F3060–F3064.
25 D. Marrocchelli, S. R. Bishop and J. Kilner, J. Mater. Chem. A, 2013, **1**, 7673.
26 P. H. Larsen, P. V. Hendriksen and M. Mogensen, J. Therm. Anal., 1997, **49**, 1263–1275.
27 T. R. Armstrong, J. W. Stevenson, L. R. Pederson and P. E. Raney, J. Electrochem. Soc., 1996, **143**, 2919–2925.
28 Mori, K, K. Miyamoto, Takenobu, K and T. Matsudaira, Oslo, vol. 2, p. 541.
29 Mori, K, K. Miyamoto, Takenobu, K and T. Matsudaira, in The Electrochemical Society, vol. 97, p. 1301.
30 D. Marrocchelli, C. Chatzichristodoulou and S. R. Bishop, Phys. Chem. Chem. Phys., 2014, **16**, 9229–9232.
31 X. Chen and T. Grande, Chem. Mater., 2013, **25**, 927–934.
32 N. H. Perry, S. Bishop and H. L. Tuller, J. Mater. Chem. A, 2014.
33 N. H. Perry, J. E. Thomas, D. Marrocchelli, S. R. Bishop and H. L. Tuller, ECS Trans., 2013, **57**, 1879–1884.
34 A. Y. Zuev, V. V. Sereda and D. S. Tsvetkov, J. Electrochem. Soc., 2012, **159**, F594–F599.
35 S. R. Bishop, K. L. Duncan and E. D. Wachsman, Electrochimica Acta, 2009, **54**, 1436–1443.
36 S. J. Hong and A. V. Virkar, J. Am. Ceram. Soc., 1995, **78**, 433–439.
37 J.-C. Grenier, N. Ea, M. Pouchard and P. Hagenmuller, J. Solid State Chem., 1985, **58**, 243–252.
38 M. Schmidt and S. J. Campbell, J. Solid State Chem., 2001, **156**, 292–304.
39 Y. Kuru, D. Marrocchelli, S. R. Bishop, D. Chen, B. Yildiz and H. L. Tuller, J. Electrochem. Soc., 2012, **159**, F799–F803.
40 S. R. Bishop, T. Nakamura and K. Amezawa, Solid State Ion., 2014, **261**, 1–4.
41 G. Kresse and J. Furthmüller, Phys. Rev. B, 1996, **54**, 11169–11186.
42 M. Burbano, D. Marrocchelli, B. Yildiz, H. L. Tuller, S. T. Norberg, S. Hull, P. A. Madden and G. W. Watson, J. Phys. Condens. Matter, 2011, **23**, 255402.
43 D. Marrocchelli, M. Salanne, P. A. Madden, C. Simon and P. Turq, Mol. Phys., 2009, **107**, 443–452.
44 M. Salanne, D. Marrocchelli and G. W. Watson, J. Phys. Chem. C, 2012, **116**, 18618–18625.
45 S. T. Norberg, I. Ahmed, S. Hull, D. Marrocchelli and P. A. Madden, J. Phys. Condens. Matter, 2009, **21**, 215401.
46 M. Burbano, S. T. Norberg, S. Hull, S. G. Eriksson, D. Marrocchelli, P. A. Madden and G. W. Watson, Chem. Mater., 2012, **24**, 222–229.
47 G. J. Martyna, D. J. Tobias and M. L. Klein, J. Chem. Phys., 1994, **101**, 4177–4189.
48 G. J. Martyna, M. L. Klein and M. Tuckerman, J. Chem. Phys., 1992, **97**, 2635–2643.
49 D. Marrocchelli, P. A. Madden, S. T. Norberg and S. Hull, Chem. Mater., 2011, **23**, 1365–1373.
50 P. Datta, P. Majewski and F. Aldinger, J. Alloys Compd., 2007, **438**, 232–237.
51 A. Skowron, P. Huang and A. Petric, J. Solid State Chem., 1999, **143**, 202–209.
52 M. S. Islam and R. A. Davies, J. Mater. Chem., 2004, **14**, 86.
53 T. L. Nguyen, M. Dokiya, S. Wang, H. Tagawa and T. Hashimoto, Solid State Ion., 2000, **130**, 229–241.
54 N. H. Perry, J. J. Kim, S. R. Bishop and H. L. Tuller, J. Mater. Chem. A, 2015, **3**, 3602–3611.
55 R. D. Shannon and C. T. Prewitt, Acta Crystallogr. B, 1969, **25**, 925–946.
56 D. Lybye, F. W. Poulsen and M. Mogensen, Solid State Ion., 2000, **128**, 91–103.
57 V. V. Kharton, A. A. Yaremchenko, M. V. Patrakeev, E. N. Naumovich and F. M. B. Marques, J. Eur. Ceram. Soc., 2003, **23**, 1417–1426.
58 T.-Y. Chen and K.-Z. Fung, J. Alloys Compd., 2004, **368**, 106–115.
59 A. S. Verma and V. K. Jindal, J. Alloys Compd., 2009, **485**, 514–518.
60 R. L. Moreira and A. Dias, J. Phys. Chem. Solids, 2007, **68**, 1617–1622.
61 L. Q. Jiang, J. K. Guo, H. B. Liu, M. Zhu, X. Zhou, P. Wu and C. H. Li, J. Phys. Chem. Solids, 2006, **67**, 1531–1536.
62 R. Ubic and G. Subodh, J. Alloys Compd., 2009, **488**, 374–379.
63 A. Y. Zuev, V. V. Sereda and D. S. Tsvetkov, J. Electrochem. Soc., 2014, **161**, F3032–F3038.
64 J. T. S. Irvine and P. Connor, Solid Oxide Fuels Cells: Facts and Figures - Past Present and Future Perspectives for SOFC Technologies, Springer.
65 N. H. Perry, D. Pergolesi, S. R. Bishop and H. L. Tuller, Solid State Ion.

